Structural Engineering and Mechanics, *Vol. 68, No. 3 (2018) 313-323*
DOI: https://doi.org/10.12989/sem.2018.68.3.313

Thermally induced mechanical analysis of temperature-dependent FG-CNTRC conical shells

Jalal Torabi* and Reza Ansari**

Department of Mechanical Engineering, University of Guilan, P.O. Box 3756, Rasht, Iran

(Received March 5, 2018, Revised September 3, 2018, Accepted September 8, 2018)

Abstract. A numerical study is performed to investigate the impacts of thermal loading on the vibration and buckling of functionally graded carbon nanotube-reinforced composite (FG-CNTRC) conical shells. Thermo-mechanical properties of constituents are considered to be temperature-dependent. Considering the shear deformation theory, the energy functional is derived, and applying the variational differential quadrature (VDQ) method, the mass and stiffness matrices are obtained. The shear correction factors are accurately calculated by matching the shear strain energy obtained from an exact three-dimensional distribution of the transverse shear stresses and shear strain energy related to the first-order shear deformation theory. Numerical results reveal that considering temperature-dependent material properties plays an important role in predicting the thermally induced vibration of FG-CNTRC conical shells, and neglecting this effect leads to considerable overestimation of the stiffness of the structure.

Keywords: FG-CNTRC conical shells; vibration and buckling; variational formulation; thermal loading

1. Introduction

Since their discovery by Iijima (1991), carbon nanotubes (CNTs) have attracted a great research interest in many areas of science and technology. Superior mechanical, thermal and electrical properties of CNTs (Yakobson and Avouris 2001, Ho *et al.* 2004, Manchado *et al.* 2005, Sumfleth 2010) make them an excellent candidate for the reinforcement of polymer composites (Esawi and Farag 2007, Fiedler *et al.* 2006). Since the nanotubes are distributed uniformly or randomly in the traditional carbon nanotube-reinforced composites (CNTRCs), mechanical properties of these kinds of composites do not vary spatially. On the other hand, functionally graded materials (FGMs) are the new generation of inhomogeneous composites in which the material properties are smoothly and continuously varied in the preferred direction. Employing the concept of FGMs, the pattern of the functionally graded (FG) distribution of reinforcement has been successfully used for functionally graded carbon nanotube-reinforced composites. For the first time, Shen (2009) studied the nonlinear bending of FG-CNTRC plates and showed that mechanical behavior of CNTRCs could be significantly improved via functionally graded distribution of CNTs within an isotropic matrix.

Besides the analytical approaches (Xiang *et al.* 2002, Sofiyev *et al.* 2003, Sofiyev *et al.* 2017a, Sofiyev *et al.* 2017b, Jin *et al.* 2013), various numerical approaches such as finite element method (FEM), mesh-free method, generalized differential quadrature (GDQ) method, harmonic differential quadrature (HDQ) method and discrete singular convolution (DSC) method, have been widely used to analyze the static and dynamic analysis of composite and functionally graded materials (Liew *et al.* 2004, Civalec 2008, Gürses *et al.* 2009, Baltacıoglu *et al.* 2010, Civalec *et al.* 2010, Baltacıoglu *et al.* 2011, Talebitooti 2013). For instance, Sofiyev *et al.* (2017a) studied the thermoelastic buckling of FGM conical shells subjected to the non-linear temperature rise based on the shear deformation theory. The Galerkin method was employed to find the non-linear thermal buckling load. In addition, Gürses *et al.* (2009) presented the free vibration analysis of laminated skew plates based on Mindlin's plate theory using the DSC technique. Civalec (2008) also employed the DSC method for the static analysis of cross-ply laminated rectangular Mindlin plates based on the first-order shear deformation theory. Furthermore, the three-dimensional free vibration of rotating laminated conical shells was investigated by Talebitooti (2013) using the layerwise DQ method.

In recent years, many theoretical investigations have been carried out on the mechanical behavior of functionally graded carbon nanotube-reinforced composite beams (Yang *et al.* 2015, Ansari *et al.* 2017a, Rafiee 2013) and plates (Shen and Zhang 2010, Ansari *et al.* 2017b, Kiani 2016). Mechanical behaviors of functionally graded CNT-reinforced composite panels and shells have been also studied by many researchers. Yas *et al.* (2013) investigated the vibration of simply-supported FG-CNTRC cylindrical panels based on the three-dimensional theory of elasticity. Mehrabadi and Aragh (2014) studied the bending behavior of FG-CNTRC cylindrical panels under mechanical loadings. The governing equations were derived based on

*Corresponding author
E-mail: Jalal.torabii@gmail.com
**Corresponding author, Ph.D.
E-mail: R_ansari@guilan.ac.ir

http://www.techno-press.com/journals/sem&subpage=7
ISSN: 1225-4568 (Print), 1598-6217 (Online)

the third-order shear deformation theory (TSDT) and were discretized by employing the two-dimensional GDQ method along with the trigonometric functions.

Shen and Xiang (2014) examined the thermal effects on nonlinear vibration behavior of FG-CNTEC cylindrical panels embedded in elastic foundations. The material properties of CNTRCs were assumed to be temperature-dependent. The equations of motion were solved by use of perturbation technique to determine the nonlinear frequencies of the CNTRC panels. Shen and Xiang (2015) studied the thermal postbuckling of CNTRC cylindrical panels embedded in elastic foundations. A singular perturbation technique combined with a two-step perturbation approach was employed to determine the buckling loads and postbuckling equilibrium paths. Also, aerothermoelastic properties and active flutter control of CNTRC panels were investigated by Zhang *et al.* (2016) in supersonic airflow. The governing equations were presented based on Reddy's third-order shear deformation theory. Employing the displacement feedback algorithm, the controller was designed and in order to study the aerothermoelastic properties and active flutter control effects of the panels, the frequency domain method was considered.

Hosseini (2013) examined the vibration of FG-CNTRC cylindrical shells using hybrid mesh-free method based on generalized finite difference (GFD) method. Nonlinear vibration of FG-CNTRC cylindrical shells was examined by Shen and Xiang (2012). Furthermore, thermal postbuckling analysis of FG-CNTRC cylindrical shells was presented by Shen (2012). In these studies, the higher-order shear deformation theory with a von Kármán-type of kinematic nonlinearity was used to derive the governing equations.

Also, there are some studies on the mechanical behaviors of FG-CNTRC conical shells. For example, Heydarpour *et al.* (2014) studied the free vibration of rotating FG-CNTRC truncated conical shells. Using Hamilton's principle and based on the first-order shear deformation theory (FSDT) of shells, the governing equations were derived and solved by means of GDQ method. Kiani (2016) investigated the torsional vibration of nanocomposite conical shells reinforced with single-walled carbon nanotubes (SWCNTs). Using the concept of Hamilton's principle and based on the Donnell's shell theory in conjunction with the first-order shear deformation shell theory, the motion equations were derived. Furthermore, Ansari and Torabi (2016) analyzed the buckling and vibration of FG-CNTRC conical shells under axial mechanical loading. The governing equations were presented based on the first-order shear deformation theory, and the numerical approach was employed to solve the problem. Also, Mirzaei and Kiani (2015) investigated the linear thermal buckling of CNTRC conical shells. The stability equations were derived based on the first-order shear deformation shell theory, Donnell kinematic assumptions and von Kármán type of geometrical nonlinearity.

This paper deals with the buckling and vibration of thermally pre-stressed FG-CNTRC conical shells using the VDQ method. The main focus is on the analyzing the effect of thermal loading on the vibrational characteristics and buckling behavior of such shells considering the temperature-dependent material properties. The physical properties of FG-CNTRC materials are assumed to be graded throughout the thickness direction and are estimated via the rule of mixture. On the basis of the first-order shear deformation theory and using Sander's strain-displacement relations, the energy functional of the nanocomposite conical shell is presented. Employing the GDQ and periodic differential operators in axial and circumferential direction, respectively, the energy functional is directly discretized based on the VDQ method. Note that in accordance with the VDQ method, one does not need to derive the analytical governing differential equations of the strong form. In addition, VDQ provides an alternative way to discretize the energy functional, which avoids the local interpolation and the assembly process usually used in FEM. Comparison of the efficiency of the VDQ with some other numerical approaches were presented by Shojaei and Ansari (2017). In addition, using matrix relations and based on Hamilton's principle, the reduced forms of mass and stiffness matrices are obtained from the discretized form of variational formulation. It is worth to note that applying the periodic differential operators in circumferential direction, one does not need to satisfy the periodicity condition in numerical differential operators. The accuracy of the present method is compared with the results given in the literature. Furthermore, the influences of volume fraction of CNT, different types of distribution of CNT through the thickness direction and various geometrical parameters on thermal stability and vibration behavior of FG-CNTRC conical shells are studied. Also, both temperature-dependent and temperature-independent results are reported to reveal the significance of temperature dependency.

2. Functionally graded carbon nanotube-reinforced composites

It is assumed that the CNTRC is made of a mixture of SWCNTs and isotropic matrix in which material properties are varied continuously throughout the thickness direction. In addition to uniform distribution (UD) of CNTs along the thickness of CNTRC conical shell, three types of functionally graded distributions of CNTs are considered which are denoted by FGA, FGO and FGX. In the case of FGA type, the inner surface of the shell is CNT-rich while for FGO type, the mid-plane of the shell is CNT-rich. Additionally, both inner and outer surfaces of the shell are CNT-rich for FGX type. The overall material characteristics of nanotube-reinforced composites can be expressed according to different micromechanical models. In this paper, the effective Young's and shear modulus are given on the basis of extended rule of mixture as follows (Shen 2012)

$$E_{11} = \eta_1 V_{cn} E_{11}^{cn} + V_m E^m \tag{1}$$

$$\frac{\eta_2}{E_{22}} = \frac{V_{cn}}{E_{22}^{cn}} + \frac{V_m}{E^m} \tag{2}$$

$$\frac{\eta_3}{G_{12}} = \frac{V_{cn}}{G_{12}^{cn}} + \frac{V_m}{G^m} \tag{3}$$

where E_{11}^{cn}, E_{22}^{cn} and E^m respectively denote Young's modulus of CNT and isotropic matrix. In addition, G_{12}^{cn} and G_{12}^{m} stand for shear modulus of CNT and matrix. Different studies indicated that the mechanical behavior of nano-structures is size-dependent (Lam *et al.* 2003, Akgoz and Civalek 2013, Gürses *et al.* 2012). Therefore, the coefficients η_i ($j = 1,2,3$) are introduced as the CNT efficiency parameters which capture the size-dependency of material properties and can be determined by matching the effective elastic modulus of CNTRC predicted by the molecular dynamics approach and those given by rule of mixture (Shen 2012). Furthermore, V_{cn} and V_m are the CNT and matrix volume fractions, respectively, related by $V_{cn} + V_m = 1$.

The density and thermal expansion coefficients of nanocomposite conical shell can be expressed as (Shen 2012)

$$\rho = V_{cn}\rho^{cn} + V_m\rho^m \tag{4}$$

$$\alpha_{11} = \frac{V_{cn}E_{11}^{cn}\alpha_{11}^{cn} + V_m E^m \alpha^m}{V_{cn}E_{11}^{cn} + V_m E^m} \tag{5}$$

$$\alpha_{22} = (1 + \nu_{12}^{cn})V_{cn}\alpha_{22}^{cn} + (1 + \nu^m)V_m\alpha^m - \nu_{12}\alpha_{11} \tag{6}$$

where α_{11}^{cn}, α_{22}^{cn} and α^m are thermal expansion coefficients, and ν_{12}^{cn} and ν^m are Poisson's rat1ios, of CNT and matrix phase, respectively. Also, ρ^m is the density of matrix and ρ^{cn} stand for the density of CNT. Moreover, Poisson's ratio of nanocomposite is given as

$$\nu_{12} = V_{cn}\nu_{12}^{cn} + V_m\nu^m \tag{7}$$

3. Governing equations

Consider a conical shell with the small radius R_1, large radius R_2, thickness h, semi-apex angle α and length L. The curvilinear coordinate system of x, θ and z coincides with the meridional, circumferential, and normal directions of the shell, respectively. On the basis of first-order shear deformation theory, the displacement field is defined as

$$\begin{gathered} u = u_0 + z\,\psi_0(x,\theta,t), \qquad v = v_0 + z\,\phi_0(x,\theta,t), \\ w = w_0(x,\theta,t) \end{gathered} \tag{8}$$

where u_0, v_0 and w_0 stand for displacement of a point on the natural axis along the x, θ and z direction and ψ_0 and ϕ_0 denote the rotations about θ and x directions, respectively. Eq. (8) can be written as

$$\tilde{\mathbf{U}} = \begin{bmatrix} u \\ v \\ w \end{bmatrix} = \mathbf{P_0}\mathbf{U}, \quad \mathbf{P_0} = \begin{bmatrix} 1 & 0 & 0 & z & 0 \\ 0 & 1 & 0 & 0 & z \\ 0 & 0 & 1 & 0 & 0 \end{bmatrix}, \quad \mathbf{U} = \begin{bmatrix} u_0 \\ v_0 \\ w_0 \\ \psi_0 \\ \phi_0 \end{bmatrix} \tag{9}$$

in which $\tilde{\mathbf{U}}$ is the displacement vector and $\mathbf{U}$ is the augmented displacement vector. According to displacement field the strain vector of conical shell can be given as (Tornabene *et al.* 2009)

$$\boldsymbol{\epsilon} = (\mathbf{E_1} + \mathbf{P_1}\mathbf{E_2})\,\mathbf{U} \tag{10}$$

in which

$$\begin{gathered} \boldsymbol{\epsilon} = [\boldsymbol{\epsilon}_p \quad \boldsymbol{\epsilon}_s]^{\mathrm{T}}, \qquad \boldsymbol{\epsilon}_p = [\epsilon_{11} \quad \epsilon_{22} \quad \gamma_{12}], \\ \boldsymbol{\epsilon}_s = [\,\gamma_{23} \quad \gamma_{13}] \end{gathered} \tag{11}$$

$$\mathbf{E_1} = \begin{bmatrix} \partial_x & 0 & 0 & 0 & 0 \\ \frac{\sin(\alpha)}{r(x)} & \frac{1}{r(x)}\partial_\theta & \frac{\cos(\alpha)}{r(x)} & 0 & 0 \\ \frac{1}{r(x)}\partial_\theta & \partial_x - \frac{\sin(\alpha)}{r(x)} & 0 & 0 & 0 \\ 0 & -\frac{\cos(\alpha)}{r(x)} & \frac{1}{r(x)}\partial_\theta & 0 & 1 \\ 0 & 0 & \partial_x & 1 & 0 \end{bmatrix}, \tag{12}$$

$$\mathbf{E_2} = \begin{bmatrix} 0 & 0 & 0 & \partial_x & 0 \\ 0 & 0 & 0 & \frac{\sin(\alpha)}{r(x)} & \frac{1}{r(x)}\partial_\theta \\ 0 & 0 & 0 & \frac{1}{r(x)}\partial_\theta & \partial_x - \frac{\sin(\alpha)}{r(x)} \\ 0 & 0 & 0 & 0 & 0 \\ 0 & 0 & 0 & 0 & 0 \end{bmatrix}, \tag{13}$$

$$\mathbf{P_1} = \mathrm{diag}([z \quad z \quad z \quad 0 \quad 0]) \tag{14}$$

where $r(x) = R_1 + x\sin(\beta)$. $\boldsymbol{\epsilon}$ is the strain vector and $\mathbf{E_1}$ and $\mathbf{E_2}$ are the strain matrix operators. In accordance to the strain vector, the stress vector can be given as

$$\begin{gathered} \boldsymbol{\sigma} = [\boldsymbol{\sigma}_p \quad \boldsymbol{\sigma}_s]^{\mathrm{T}}, \qquad \boldsymbol{\sigma}_p = [\sigma_{11} \quad \sigma_{22} \quad \tau_{12}], \\ \boldsymbol{\sigma}_s = [\,\tau_{23} \quad \tau_{13}] \end{gathered} \tag{15}$$

Additionally, based on Hook's law, the stress-strain relation is presented as

$$\boldsymbol{\sigma} = \mathbf{C}\boldsymbol{\epsilon} \tag{16}$$

in which

$$\begin{gathered} \mathbf{C} = \begin{bmatrix} \mathbf{C}_p & \mathbf{0}_{3\times 2} \\ \mathbf{0}_{2\times 3} & \mathbf{C}_s \end{bmatrix}, \qquad \mathbf{C}_p = \begin{bmatrix} Q_{11} & Q_{12} & 0 \\ Q_{21} & Q_{22} & 0 \\ 0 & 0 & Q_{66} \end{bmatrix}, \\ \mathbf{C}_s = \begin{bmatrix} Q_{44} & 0 \\ 0 & Q_{55} \end{bmatrix} \end{gathered} \tag{17}$$

where

$$\begin{gathered} Q_{11} = \frac{E_{11}}{1 - \nu_{12}\nu_{21}}, \qquad Q_{22} = \frac{E_{22}}{1 - \nu_{12}\nu_{21}}, \\ Q_{12} = \frac{\nu_{21}E_{11}}{1 - \nu_{12}\nu_{21}}, \\ Q_{44} = G_{23}, \qquad Q_{55} = G_{13}, \qquad Q_{66} = G_{12}. \end{gathered} \tag{18}$$

Now, the governing equations are presented using Hamilton's principle. For this account, the strain energy and kinetic energy are first presented. By the use of strain and stress vector given in Eqs. (10) and (16), the elastic strain energy can be given as

$$U_e = \frac{1}{2}\int_{\forall} \boldsymbol{\epsilon}^{\mathrm{T}}\boldsymbol{\sigma} d\forall = \frac{1}{2}\int_{\forall} \boldsymbol{\epsilon}^{\mathrm{T}}\mathbf{C}\boldsymbol{\epsilon} d\forall$$
$$= \frac{1}{2}\int_A \mathbf{U}^{\mathrm{T}}\big(\mathbf{E_1^T C_1 E_1} + \mathbf{E_1^T C_2 E_2} + \mathbf{E_2^T C_2 E_1} + \mathbf{E_2^T C_3 E_2}\big)\mathbf{U} dA \tag{19}$$

where A is the cross-section area and $dA = (R_1 + x\sin(\beta))dxd\theta$. In addition

$$\mathbf{C_1} = \int_{-\frac{h}{2}}^{\frac{h}{2}} \mathbf{C} dz = \begin{bmatrix} \hat{\mathbf{C}}_p & \mathbf{0}_{3\times 2} \\ \mathbf{0}_{2\times 3} & \hat{\mathbf{C}}_s \end{bmatrix},$$
$$\mathbf{C_2} = \int_{-h/2}^{h/2} \mathbf{C}\mathbf{P_1} dz, \qquad \mathbf{C_3} = \int_{-h/2}^{h/2} \mathbf{P_1}\mathbf{C}\mathbf{P_1} dz \tag{20}$$

in which

$$\hat{\mathbf{C}}_p = \int_{-h/2}^{h/2} \begin{bmatrix} Q_{11} & Q_{12} & 0 \\ Q_{21} & Q_{22} & 0 \\ 0 & 0 & Q_{66} \end{bmatrix} dz, \tag{21}$$

$$\hat{\mathbf{C}}_s = \begin{bmatrix} \kappa_{11}\hat{C}_{s_{11}} & 0 \\ 0 & \kappa_{22}\hat{C}_{s_{22}} \end{bmatrix}, \qquad \hat{C}_{s_{ij}} = \int_{-h/2}^{h/2} C_{s_{ij}} dz, \quad (ij = 11{,}22) \tag{22}$$

In the above equation, $C_{s_{ij}}$ are the components of $\mathbf{C}_s$ presented in Eq. (17). In addition, κ_{11} and κ_{22} denote the shear correction factors in the first-order shear deformation theory. As known, the shear correction factors depend on the true stress distribution through the thickness and can be determined by matching the shear strain energy obtained from the first-order shear deformation theory and the strain energy due to the true transverse stresses predicted by the 3-D elasticity theory (Oñate 2013), as presented in the Appendix.

Moreover, according to displacement field given in Eq. (9), the kinetic energy can be presented as

$$T = \frac{1}{2}\int_A \dot{\mathbf{U}}^{\mathrm{T}}\boldsymbol{\rho}\dot{\mathbf{U}} dA, \qquad \boldsymbol{\rho} = \int_A \mathbf{P_0^T}\rho\mathbf{P_0} \mathrm{d}z \tag{23}$$

In addition, the strain energy due to initial thermal loading can be calculated as

$$U_T = \frac{1}{2}\int_A \mathbf{U}^{\mathrm{T}}\mathbf{Q}^{\mathrm{T}}\mathbf{G}\mathbf{Q}\mathbf{U} dA \tag{24}$$

where

$$\mathbf{Q} = \begin{bmatrix} 0 & 0 & \dfrac{\partial}{\partial x} & 0 & 0 \\ 0 & 0 & \dfrac{1}{r(x)}\dfrac{\partial}{\partial \theta} & 0 & 0 \end{bmatrix}, \tag{25}$$

$$\mathbf{G} = \begin{bmatrix} N_x^0 & \dfrac{N_{x\theta}^0}{2} \\ \dfrac{N_{x\theta}^0}{2} & N_\theta^0 \end{bmatrix} \tag{26}$$

in which N_x^0, N_θ^0 and $N_{x\theta}^0$ are force resultants due to initial thermal loading in pre-buckling state. Since the deformation of the structure is small in pre-buckling state, one can obtain these force resultants considering membrane solution of linear equilibrium equations as (Torabi *et al.* 2013, Akbari *et al.* 2015)

$$N_x^0 = -\frac{(\mathcal{A}_{22}N_x^T - \mathcal{A}_{12}N_\theta^T)\sin(\alpha)\, L}{r(x)\,\mathcal{A}_{22}\ln\left(1 + \dfrac{L\sin(\alpha)}{R_1}\right)}, \quad N_\theta^0 = 0, \quad N_{x\theta}^0 = 0. \tag{27}$$

where

$$\begin{Bmatrix} N_x^T \\ N_\theta^T \end{Bmatrix} = \int_{-\frac{h}{2}}^{\frac{h}{2}} \begin{bmatrix} Q_{11} & Q_{12} \\ Q_{12} & Q_{22} \end{bmatrix} \begin{Bmatrix} \alpha_{11} \\ \alpha_{22} \end{Bmatrix} \Delta T(z)\, dz \tag{28}$$

In the above equation, $\Delta T(z)$ is the temperature rise from reference temperature. Considering the strain energy and kinetic energy, the Hamilton's principle is defined as

$$\int_{t_1}^{t_2} \delta(T - U)dt = 0 \tag{29}$$

It should be noted that in the present study, the strain energy (U) is due to elastic strain energy (U_e) and initial thermal loading (U_T) i.e., $U = U_e + U_T$. Accordingly, substituting Eqs. (19), (23) and (24) into the Hamilton's principle results in

$$\int_{t_1}^{t_2} \delta \int_A \Big(\frac{1}{2}\dot{\mathbf{U}}^{\mathrm{T}}\boldsymbol{\rho}\dot{\mathbf{U}} - \frac{1}{2}\mathbf{U}^{\mathrm{T}}\big(\mathbf{E_1^T C_1 E_1} + \mathbf{E_1^T C_2 E_2} + \mathbf{E_2^T C_2 E_1} + \mathbf{E_2^T C_3 E_2}\big)\mathbf{U} - \frac{1}{2}\mathbf{U}^{\mathrm{T}}\mathbf{Q}^{\mathrm{T}}\mathbf{G}\mathbf{Q}\mathbf{U}\Big) dAdt \tag{30}$$

The energy functional of the system presented in Eq. (30) can be directly discretized using VDQ method (Shojaei and Ansari 2017, Ansari *et al.* 2016). On the other word, according to the VDQ approach, the displacement vector and its derivatives appeared in the strain vector are discretized employing the numerical differential and integral operators. Following the numerical discretization procedure explained in (Shojaei and Ansari 2017), the discretized form of Eq. (30) is given as

$$\int_{t_1}^{t_2} \delta \Big(\frac{1}{2}\dot{\mathbb{U}}^{\mathrm{T}}(\boldsymbol{\rho}\otimes\mathbb{S})\dot{\mathbb{U}} - \frac{1}{2}\mathbb{U}^{\mathrm{T}}\big(\mathbb{E}_1^{\mathrm{T}}\mathbb{C}_1\mathbb{E}_1 + \mathbb{E}_1^{\mathrm{T}}\mathbb{C}_2\mathbb{E}_2 + \mathbb{E}_2^{\mathrm{T}}\mathbb{C}_2\mathbb{E}_1 + \mathbb{E}_2^{\mathrm{T}}\mathbb{C}_3\mathbb{E}_2\big)\mathbb{U} - \frac{1}{2}\mathbb{U}^{\mathrm{T}}\mathbb{Q}^{\mathrm{T}}\mathbb{G}\mathbb{Q}\mathbb{U}\Big) dt \tag{31}$$

Taking the variation and integrating by parts in time domain results in (Shojaei and Ansari 2017)

$$\mathbb{M}\ddot{\mathbb{U}} + \mathbb{K}\mathbb{U} + \mathbb{K}_{\mathbb{g}}\mathbb{U} = \mathbf{0} \tag{32}$$

Table 1 Material properties of SWCNT at particular temperatures (Shen 2012)

T [K]	E_{11}^{cn}[TPa]	E_{22}^{cn}[TPa]	G_{12}^{cn}[TPa]	ν_{12}^{cn}	$\alpha_{11}^{cn}[10^{-6}/K]$	$\alpha_{22}^{cn}[10^{-6}/K]$
300	5.6466	7.0800	1.9445	0.175	3.4584	5.1682
400	5.5679	6.9814	1.9703	0.175	4.1496	5.0905
500	5.5308	6.9348	1.9643	0.175	4.5361	5.0189
700	5.4744	6.8641	1.9644	0.175	4.6677	4.8943

where the mass matrix $\mathbb{M}$, stiffness matrix $\mathbb{K}$ and geometrical stiffness matrix $\mathbb{K}_{\mathbb{g}}$ are given as follows

$$\begin{gathered}\mathbb{M} = \boldsymbol{\rho} \otimes \mathbb{S} \\ \mathbb{K} = \mathbb{E}_1^{\mathrm{T}}\mathbb{C}_1\mathbb{E}_1 + \mathbb{E}_1^{\mathrm{T}}\mathbb{C}_2\mathbb{E}_2 + \mathbb{E}_2^{\mathrm{T}}\mathbb{C}_2\mathbb{E}_1 + \mathbb{E}_2^{\mathrm{T}}\mathbb{C}_3\mathbb{E}_2 \\ \mathbb{K}_{\mathbb{g}} = \mathbb{Q}^{\mathrm{T}}\mathbb{G}\mathbb{Q}\end{gathered} \tag{33}$$

with

$$\begin{gathered}\mathbb{S} = \mathbf{S}_\theta \otimes (\mathbf{S}_x\mathbf{R}) \\ \mathbb{C}_i = \mathbf{C}_i \otimes \mathbb{S}, \qquad (i = 1,2,3) \\ \mathbb{G} = \mathbf{G} \otimes \mathbb{S}\end{gathered} \tag{34}$$

where $\mathbf{S}_\theta$ and $\mathbf{S}_x$ are the integral operators in circumferential and axial direction, respectively and sign $\otimes$ presents the Kronecker product. Furthermore, $\mathbb{E}_1$, $\mathbb{E}_2$ and $\mathbb{Q}$ are the discretized counterparts of $\mathbf{E}_1$, $\mathbf{E}_2$ and $\mathbf{Q}$ (Ansari and Torabi 2016). In the present study, the differential and integral operators in x direction are defined based on the GDQ method. In addition, since the displacement components are periodic in circumferential direction, the periodic differential operators are used in θ direction. For the GDQ differential operators in axial direction, the Chebyshev-Gauss-Lobatto grid point distribution was considered. For periodic differential operators in circumferential direction, the uniform distribution of grid points was considered. It is worth noting that the detailed description of these numerical differential and integral operators was explained in (Shojaei and Ansari 2017).

6. Results and discussion

Stability and vibration analysis of FG-CNTRC conical shell subjected to thermal loading were presented. In this section, the accuracy of the present study is first validated by comparing the present results and those given in the literature. Then, a comprehensive parametric study is carried out to analyze the stability and vibration behavior of thermally induced CNTRC conical shell. It is assumed that the matrix phase of shell is made of Poly (methyl methacrylate) (PMMA) which its material properties are (Shen 2012): $E^m = (3.52 - 0.0034T)$ GPa, $\rho^m = 1150\ \mathrm{Kg/m^3}$, $\alpha^m = 45(1 + 0.0005\Delta\mathrm{T}) \times 10^{-6}\ 1/\mathrm{K}$ and $\nu^m = 0.34$. To calculate the elasticity modulus of the matrix $T = \Delta T + T_0$ where $T_0 = 300$ K is the reference temperature. Furthermore, (10,10) SWCNT is selected for reinforcement. The material properties of SWCNT are considerably temperature-dependent. In this regard, Shen (2012) presented the mechanical and thermal properties of SWCNT at four different temperatures including $T = 300, 400, 500$ and 700 K which are presented in Table 1. Using these values and considering a third-order interpolation, the thermo-mechanical properties of (10,10) armchair SWCNT as a function of temperature can be presented as follows

$$\begin{aligned} E_{11}^{cn}(T)[\mathrm{TPa}] &= 6.3998 - 4.338417 \times 10^{-3}T \\ &\quad + 7.43 \times 10^{-6}T \\ &\quad - 4.458333 \times 10^{-9}T^3 \\ E_{22}^{cn}(T)[\mathrm{TPa}] &= 8.02155 - 5.420375 \times 10^{3}T \\ &\quad + 9.275 \times 10^{-6}T^2 \\ &\quad - 5.5625 \times 10^{-9}T^3 \\ G_{12}^{cn}(T)[\mathrm{TPa}] &= 1.40755 + 3.476208 \times 10^{-3}T \\ &\quad - 6.965 \times 10^{-6}T^2 \\ &\quad + 4.479167 \times 10^{-9}T^3 \\ \alpha_{11}^{cn}(T)[10^{-6}/\mathrm{K}] &= -1.12515 + 0.0229169T \\ &\quad - 2.887 \times 10^{-5}T^2 \\ &\quad + 1.13625 \times 10^{-8}T^3 \\ \alpha_{22}^{cn}(T)[10^{-6}/\mathrm{K}] &= 5.43715 - 9.84625 \times 10^{-4}T \\ &\quad + 2.9 \times 10^{-7}T^2 + 1.25 \times 10^{-11}T^3 \\ \nu_{12}^{cn} &= 0.175 \\ \rho^{cn}[\mathrm{Kg/m^3}] &= 1400 \end{aligned} \tag{35}$$

Different boundary conditions such as clamped (C), simply-supported (S) and free (F) are considered at the edges of conical shell. For instance, the CS boundary condition denotes that the small and large ends of the shell are clamped and simply-supported, respectively. The essential boundary conditions at the edges of the conical shell are considered to be

$$\begin{gathered}\text{clamped:} \quad u_0 = v_0 = w_0 = \psi_0 = \phi_0 = 0, \\ \text{simply} - \text{supported:} \quad u_0 = v_0 = w_0 = \phi_0 = 0,\end{gathered} \tag{36}$$

In addition, no constraints are considered for free boundary condition. It should be noted that the uniform temperature rise is assumed along the thickness direction of the cone.

6.1 Comparison and convergence studies

The accuracy of the present study is checked by comparing the present results with those given in the literature. Firstly, the non-dimensional natural frequencies of FG-CNTRC cylindrical shell for different volume fractions and types of distribution of CNT are compared to those reported by Shen and Xiang (2012) in Table 2. Some discrepancies of the numerical results may be due to the employment of different models. In this study, the governing equations are presented based on the first-order shear deformation theory, while, the third-order shear deformation theory was used by Shen and Xiang (2012). In addition, comparison of natural frequencies of FGM conical shells for various FG power low index (k) is performed in Table 3. In the last case, by considering temperature-dependency, the buckling temperature of FG-CNTRC conical shells are compared in Table 4 with the results reported by Mirzaei and Kiani (2015). It can be seen that

Table 2 Comparison of non-dimensional natural frequency $(\Omega = \omega(R_1^2/h)\sqrt{\rho^m/E^m})$ of FG-CNTRC cylindrical shell $(h = 5\ \mathrm{mm}, \beta = 0.001, R_1/h = 10)$

1		$L = \sqrt{100R_1h}$		$L = \sqrt{500R_1h}$	
		Present study	Shen and Xiang (2012)	Present study	Shen and Xiang (2012)
0.12	UD	3.3656	3.3704	1.7020	1.7231
	FGA	3.2019	3.1568	1.6614	1.6652
	FGX	3.5674	3.6150	1.6977	1.7814
0.17	UD	4.2870	4.2866	2.1900	2.2106
	FGA	4.1155	4.0412	2.1486	2.1477
	FGX	4.5410	4.6106	2.1913	2.3121
0.28	UD	4.6543	4.6766	2.3178	2.3548
	FGA	4.5410	4.4886	2.3228	2.3306
	FGX	5.2014	5.2173	2.3675	2.5651

Table 3 Comparison of natural frequency $f = \omega/2\pi$ (Hz) of CF FGM conical shell $(\beta = 40, L\cos(\beta) = 2\ \mathrm{m}‹\ R_1 = 0.5\ \mathrm{m}, h = 0.1\ \mathrm{m})$

Mode No.	$k = 0$		$k = 1$		$k = 5$	
	Present study	Tornabene *et al.* (2009)	Present study	Tornabene *et al.* (2009)	Present study	Tornabene *et al.* (2009)
1	209.9	210.0	204.4	204.9	203.5	203.9
2	209.9	210.0	204.4	204.9	203.5	203.9
3	231.9	232.0	224.0	224.4	227.3	227.7
4	231.9	232.0	224.0	224.4	227.3	227.7
5	287.5	287.5	276.2	276.7	283.8	284.3
6	287.5	287.5	276.2	276.7	283.8	284.3
7	322.5	322.6	315.7	316.3	309.0	309.6
8	322.5	322.6	315.7	316.3	309.0	309.6
9	356.9	357.0	346.8	347.7	346.3	347.1
10	356.9	357.0	346.8	347.7	346.3	347.1

Table 4 Comparison of buckling temperature $T_{cr}(K)$ of FG-CNTRC conical shells ($\beta = 30^\circ, R_1/h = 50, L = \sqrt{100R_1h}, h = 1\ \mathrm{mm}$)

V_{cn}^*		UD	FGA	FGO	FGX
0.12	Present study	406.50	391.39	385.60	427.66
	Mirzaei and Kiani (2015)	407.75	391.77	385.82	428.07
0.17	Present study	414.71	399.54	392.97	436.84
	Mirzaei and Kiani (2015)	415.95	399.99	393.49	437.41
0.28	Present study	398.02	384.86	375.89	422.04
	Mirzaei and Kiani (2015)	399.58	385.58	376.41	422.83

the results have good agreement with those given in the literature. Furthermore, the convergence studies of the buckling temperature and non-dimensional natural frequencies of FG-CNTRC conical shells are reported in Tables 5 and 6, respectively. In this regard, variations of the buckling temperature and non-dimensional natural frequencies were presented for different number of grid points in axial (n_x) and circumferential (n_θ) directions. As

Table 5 Convergence study for the buckling temperature $T_{cr}(K)$ of SS FG-CNT conical shell $(h = 5\ \mathrm{mm}, R_1/h = 40, \beta = 30^\circ, L/R_1 = 2)$

n_θ	n_x	$V_{cn}^* = 0.12$				$V_{cn}^* = 0.28$			
		UD	FGA	FGO	FGX	UD	FGA	FGO	FGX
8	5	442.366	440.736	430.726	454.507	426.045	426.915	417.443	441.544
	7	441.628	438.178	428.083	454.041	425.557	425.756	415.585	441.218
	9	441.591	437.985	427.955	454.020	425.533	425.597	415.492	441.202
	11	441.592	437.991	427.948	454.022	425.534	425.601	415.490	441.203
	13	441.593	437.992	427.950	454.022	425.535	425.602	415.491	441.203
	15	441.593	437.992	427.951	454.022	425.535	425.603	415.491	441.204
10	5	411.937	410.687	400.477	424.787	399.691	400.966	389.137	415.843
	7	411.491	409.251	399.677	424.370	399.315	399.949	388.504	415.496
	9	411.476	409.191	399.640	424.359	399.304	399.900	388.478	415.487
	11	411.476	409.194	399.640	424.360	399.304	399.903	388.479	415.488
	13	411.477	409.194	399.641	424.360	399.305	399.903	388.479	415.488
	15	411.477	409.195	399.641	424.360	399.305	399.903	388.479	415.488
12	5	402.510	401.264	390.354	416.213	391.581	392.671	378.746	409.504
	7	402.258	400.234	390.110	415.901	391.331	391.845	378.496	409.224
	9	402.251	400.209	390.092	415.895	391.325	391.825	378.483	409.220
	11	402.252	400.211	390.093	415.895	391.326	391.827	378.484	409.220
	13	402.252	400.211	390.093	415.896	391.326	391.827	378.484	409.220
	15	402.252	400.211	390.093	415.896	391.326	391.827	378.484	409.220
14	5	402.510	401.264	390.354	416.213	391.581	392.671	378.746	409.504
	7	402.258	400.234	390.110	415.901	391.331	391.845	378.496	409.224
	9	402.251	400.209	390.092	415.895	391.325	391.825	378.483	409.220
	11	402.252	400.211	390.093	415.895	391.326	391.827	378.484	409.220
	13	402.252	400.211	390.093	415.896	391.326	391.827	378.484	409.220
	15	402.252	400.211	390.093	415.896	391.326	391.827	378.484	409.220

observed, the numerical results rapidly converge with the increase of the number of grid points.

6.2 Parametric study

The accuracy of the present study was verified by the results given in the literature in the previous section. Here, some numerical results are conducted to investigate the effects of involved parameters on stability and vibration behavior of FG-CNTRC conical shells.

Table 7 presents the variations of buckling temperature of FG-CNTRC conical shells for different values of volume fractions and types of distribution of CNTs, semi-vertex angles and length-to-small radius ratios. The boundary conditions of the shell are considered to be simply-supported at both ends. To show the importance of temperature-dependency, both temperature-dependent and temperature-independent material properties are taken into account. It can be seen that the conical shell with $V_{cn}^* = 0.17$ has the highest buckling temperature which is consistent with the findings reported in (Shen and Zhang 2010, Shen 2012) for thermal buckling of rectangular plates and cylindrical shells. In addition, the FGO type

Table 6 Convergence study for the non-dimensional natural frequencies of SS FG-CNTRC conical shell ($h = 5\ \mathrm{mm}, R_1/h = 40, \beta = 30^{\circ}, L/R_1 = 2$)

n_θ	n_x	$V_{cn}^* = 0.12$				$V_{cn}^* = 0.28$			
		UD	FGA	FGO	FGX	UD	FGA	FGO	FGX
8	5	9.958	9.881	9.556	10.387	13.758	13.942	13.335	14.727
	7	10.040	9.989	9.641	10.470	13.868	14.093	13.450	14.841
	9	10.040	9.989	9.640	10.470	13.868	14.093	13.450	14.841
	11	10.040	9.989	9.640	10.470	13.868	14.093	13.450	14.841
	13	10.040	9.989	9.640	10.470	13.868	14.093	13.450	14.841
	15	10.040	9.989	9.640	10.470	13.868	14.093	13.450	14.841
10	5	8.555	8.450	8.047	9.066	11.907	12.006	11.212	12.989
	7	8.622	8.542	8.115	9.133	11.996	12.135	11.305	13.084
	9	8.621	8.542	8.115	9.133	11.996	12.134	11.304	13.083
	11	8.622	8.542	8.115	9.133	11.996	12.135	11.304	13.083
	13	8.622	8.542	8.115	9.133	11.996	12.135	11.304	13.083
	15	8.622	8.542	8.115	9.133	11.996	12.135	11.304	13.083
12	5	8.110	7.991	7.529	8.682	11.322	11.380	10.399	12.565
	7	8.170	8.075	7.589	8.744	11.403	11.499	10.480	12.653
	9	8.170	8.075	7.589	8.744	11.403	11.498	10.480	12.653
	11	8.170	8.075	7.589	8.744	11.403	11.498	10.480	12.653
	13	8.170	8.075	7.589	8.744	11.403	11.498	10.480	12.653
	15	8.170	8.075	7.589	8.744	11.403	11.498	10.480	12.653
14	5	8.110	7.991	7.529	8.682	11.322	11.380	10.399	12.565
	7	8.170	8.075	7.589	8.744	11.403	11.499	10.480	12.653
	9	8.170	8.075	7.589	8.744	11.403	11.498	10.480	12.653
	11	8.170	8.075	7.589	8.744	11.403	11.498	10.480	12.653
	13	8.170	8.075	7.589	8.744	11.403	11.498	10.480	12.653
	15	8.170	8.075	7.589	8.744	11.403	11.498	10.480	12.653

Table 7 Variations of buckling temperature $T_{cr}(K)$ of SS FG-CNTRC conical shell for different semi-vertex angles and length-to-small radius ratios ($h = 5\ \mathrm{mm}, R_1/h = 50$)

	V_{cn}^*		$L/R_1 = 2$			$L/R_1 = 4$		
			$\beta = 15^{\circ}$	$\beta = 30^{\circ}$	$\beta = 45^{\circ}$	$\beta = 15^{\circ}$	$\beta = 30^{\circ}$	$\beta = 45^{\circ}$
Temperature independent	0.12	UD	438.39	409.41	382.38	417.63	387.40	365.05
		FGA	434.35	406.86	380.51	406.05	376.82	356.86
		FGO	424.08	397.30	370.90	401.70	374.46	354.30
		FGX	454.04	423.79	395.86	432.99	401.48	373.86
	0.17	UD	458.41	424.41	392.81	433.88	398.38	373.33
		FGA	448.14	421.73	391.19	420.12	387.39	364.11
		FGO	437.00	410.68	380.43	413.84	383.61	360.76
		FGX	477.18	440.91	407.76	452.32	414.36	384.45
	0.28	UD	418.20	394.49	372.27	401.27	376.60	356.48
		FGA	421.13	396.11	372.96	394.69	369.09	351.54
		FGO	406.08	381.18	359.52	386.79	363.58	346.73
		FGX	441.29	413.77	389.15	423.63	393.99	367.80
Temperature dependent	0.12	UD	403.75	386.05	368.14	391.25	371.67	355.43
		FGA	401.98	384.30	366.66	383.51	363.84	349.27
		FGO	395.51	377.50	359.39	381.09	362.10	347.21
		FGX	413.51	395.68	377.86	401.29	381.24	361.71
	0.17	UD	414.95	395.17	375.06	400.94	378.87	361.40
		FGA	411.95	393.60	373.85	392.92	371.06	354.62
		FGO	404.31	386.08	366.02	388.75	368.46	352.03
		FGX	426.02	405.77	385.50	412.42	389.77	369.16
	0.28	UD	391.03	375.98	360.78	380.42	363.89	348.74
		FGA	392.79	376.95	361.13	375.64	358.13	345.10
		FGO	382.74	366.31	350.91	370.47	354.05	341.24
		FGX	405.66	389.08	373.11	395.24	375.58	357.07

distribution results in lower buckling temperature of conical shell. In other words, the special feature of FGO type (mid-plane of the shell is CNT rich), reduces the stiffness of the structure. Furthermore, the increase in length-to-small radius ratio and semi-vertex angle of conical shell makes the structure less stable so that the buckling temperatures decrease. Also, it is concluded that considering temperature-dependent material properties plays an important role in predicting the stability of the FG-CNTRC conical shells and considerably decreases the buckling temperature.

The influences of initial thermal loading on non-dimensional natural frequency of clamped-clamped FG-CNTRC conical shell for different volume fractions and distributions of CNT are presented in Table 8. Generally, it can be seen that the increase in volume fractions of CNT increases the non-dimensional natural frequencies. It is apparent that the increase in initial thermal loading increases the deformation of the cone in prebuckling state and so decreases the natural frequency. It is worth to note that the initial thermal loading is considered as a fraction of buckling temperature difference. For example, in the case of $V_{cn}^* = 0.12$, FGX type of distribution and considering temperature-dependent material properties, the increase of initial thermal loading from $\Delta T = 0$ to $\Delta T = 3\Delta T_{cr}/4$, decreases the non-dimensional natural frequency about 37%. Furthermore, it is found that neglecting the temperature-dependent material properties overestimates the stiffness of the structure and consequently predicts higher values for buckling temperature. One can see that in the case of $V_{cn}^* = 0.12$, FGX type of distribution and $R_1/h = 20$, considering the temperature-dependent material properties, decreases the buckling temperature difference about 37%.

Considering the temperature dependency, the variations of non-dimensional natural frequencies of FG-CNTRC conical shells versus uniform temperature rise through the thickness direction are demonstrated in Figs. 1 and 2 for four boundary conditions and different values of length-to-small radius ratios and semi-vertex angles, respectively. The results show that the increase in L/R_1 and β makes the conical shells more flexible and so decreases the buckling resistance and natural frequency of the structure. Furthermore, Fig. 1 reveals that in the case of small L/R_1 (for instance $L/R_1 = 2$) increase in initial thermal loading results in swift decrease of non-dimensional natural

Table 8 Effects of initial thermal loading on non-dimensional natural frequency $\Omega = \omega(R_1^2/h)\sqrt{\rho^m/E^m}$ of CC FG-CNTRC conical shell ($h = 5$ mm$, \beta = 25^{\circ}, L/R_1 = 2, R_1/h = 20$)

	V_{cn}^*		$\Delta T = 0$	$\Delta T = \frac{\Delta T_{cr}}{4}$	$\Delta T = \frac{\Delta T_{cr}}{2}$	$\Delta T = \frac{3\Delta T_{cr}}{4}$
Temperature independent	0.12	UD (341.74)*	10.93	9.58	7.94	5.71
		FGO (241.03)	9.22	8.07	6.68	4.80
		FGX (437.70)	12.20	10.69	8.87	6.41
	0.17	UD (368.73)	13.57	11.90	9.85	7.08
		FGO (261.20)	11.48	10.05	8.32	5.99
		FGX (427.29)	15.16	13.28	11.01	7.94
	0.28	UD (318.85)	15.73	13.79	11.43	8.22
		FGO (217.62)	13.11	11.47	9.48	6.81
		FGX (413.05)	17.66	15.48	12.84	9.26
Temperature dependent	0.12	UD (226.87)	10.93	10.11	8.82	6.68
		FGO (168.07)	9.22	8.43	7.27	5.45
		FGX (275.02)	12.20	11.38	10.01	7.69
	0.17	UD (238.95)	13.57	12.59	11.00	8.35
		FGO (177.79)	11.48	10.52	9.09	6.83
		FGX (289.74)	15.16	14.17	12.49	9.62
	0.28	UD (213.45)	15.73	14.54	12.68	9.60
		FGO (155.38)	13.11	11.97	10.31	7.71
		FGX (258.47)	17.66	16.44	14.45	11.08

*Number in the parenthesis indicates the buckling temperature difference (ΔT_{cr})

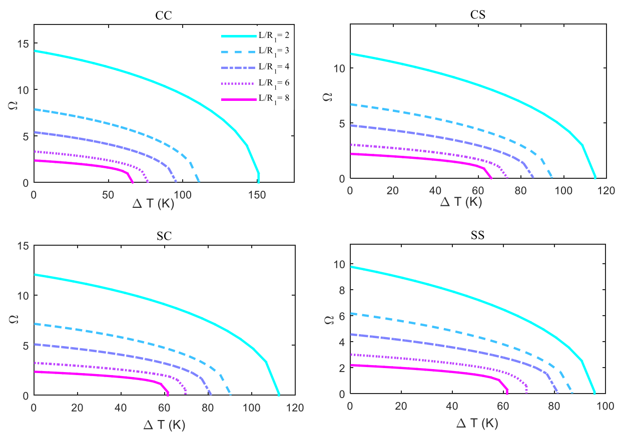

Fig. 1 Effects of initial thermal loading on non-dimensional natural frequency $\Omega = \omega(R_1^2/h)\sqrt{\rho^m/E^m}$ of FG-CNTRC conical shell for various length-to-small radius ratios and boundary conditions ($h = 5$ mm$, \beta = 30^{\circ}, \frac{R_1}{h} = 40, V_{cn}^* = 0.12$, FGX)

frequencies, whereas for the cone with larger L/R_1 (for instance $L/R_1 = 8$), the increase in temperature difference yields to gradual decrease of natural frequencies.

Moreover, Fig. 2 depicts that by increasing the semi-vertex angle, the buckling temperature differences of conical shell are more affected rather than the natural frequencies. For example, it is observed that the increase of

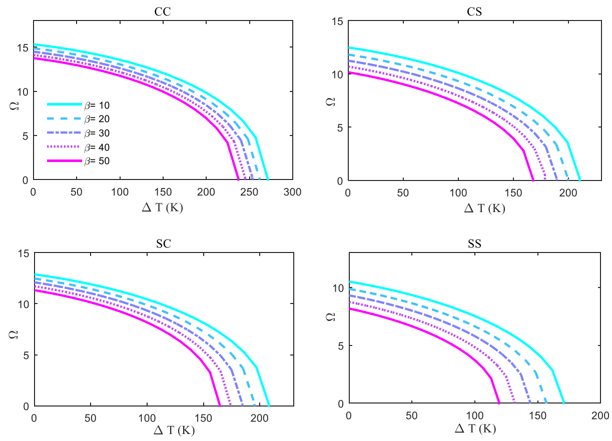

Fig. 2 Effects of initial thermal loading on non-dimensional natural frequency $\Omega = \omega(R_1^2/h)\sqrt{\rho^m/E^m}$ of FG-CNTRC conical shell for various semi-vertex angles and boundary conditions ($h = 5$ mm$, \frac{L}{R_1} = 2, \frac{R_1}{h} = 25, V_{cn}^* = 0.28$, UD)

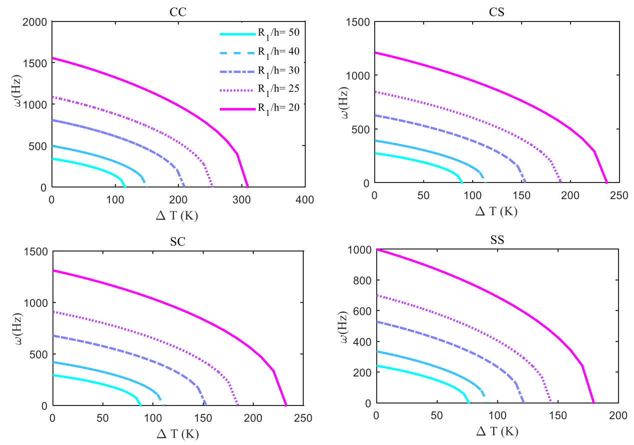

Fig. 3 Effects of initial thermal loading on natural frequency (Hz) of FG-CNTRC conical shell for various small radius-to-thickness ratios and boundary conditions ($h = 5$ mm$, \beta = 30, \frac{L}{R_1} = 2, V_{cn}^* = 0.28$, UD)

semi-vertex angle from $\beta = 10$ to $\beta = 50$, decreases the non-dimensional natural frequency about 10%, while the reduction of the buckling temperature difference is about 13%. Note that investigation of the results for different boundary conditions also reveals that the CC conical shell has the highest buckling temperature and non-dimensional natural frequencies and there are no considerable differences between CS and SC boundary conditions. Fig. 3 demonstrates the effects of initial thermal loadings on natural frequencies of FG-CNTRC conical shell for various boundary conditions and small radius-to-thickness ratios. It can be seen that thicker cones have larger buckling temperature differences and natural frequencies. In addition, comparison of different boundary conditions implies that the initial thermal loading has stronger decreasing effects on the natural frequency of SS conical shell rather than other boundary conditions.

The influences of temperature-dependency of material properties on the thermally induced vibration analysis of

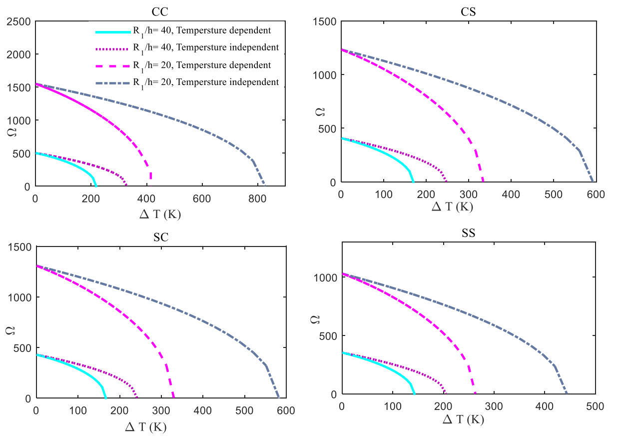

Fig. 4 Effects of considering the temperature-dependent material properties on the thermally induced vibration of FG-CNTRC conical shell ($h = 5\,\text{mm}, \beta = 20, \frac{L}{R_1} = 2, V_{cn}^* = 0.17, \text{FGX}$)

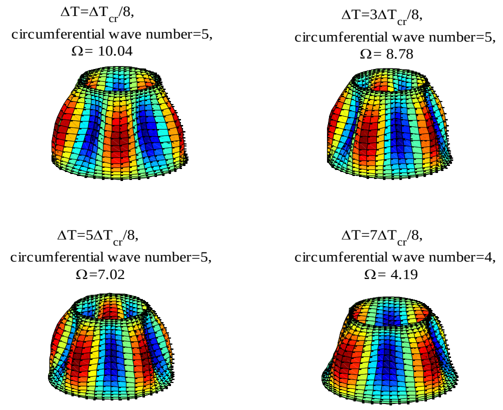

Fig. 5 Effects of initial thermal loading on the fundamental vibrational mode shapes of simply-supported FG-CNTRC conical shell ($\beta = 20^{\circ}, \frac{L}{R_1} = 2, \frac{R_1}{h} = 50, V_{cn}^* = 0.12, \text{FGX}$)

FG-CNTRC conical shells are demonstrated in Fig. 4. In this figure, by considering both temperature-dependent and temperature-independent material properties, the non-dimensional natural frequencies versus initial thermal loading are presented for two different radius-to-thickness ratios. As it can be seen, considering the temperature-dependent material properties has considerable effects on the natural frequencies of thermally induced FG-CNTRC conical shells. In addition, one can see that the effects of temperature-dependent materials are more significant for the shells with smaller radius-to-thickness ratio.

In addition, the influences of initial thermal loading on the fundamental vibrational mode shapes of FG-CNTRC conical shells are illustrated in Fig. 5. The thermal loadings are considered as the fraction of the critical buckling temperature difference. As observed, for $\Delta T = \Delta T_{cr}/8$, $\Delta T = 3\Delta T_{cr}/8$ and $\Delta T = 5\Delta T_{cr}/8$, the fundamental vibrational mode shape has five circumferential wave numbers, while by the increase of initial thermal loading to $\Delta T = 7\Delta T_{cr}/8$, the fundamental vibrational mode shape has four circumferential wave numbers.

7. Conclusions

Thermal buckling and vibration analysis of thermally induced FG-CNTRC conical shells were presented employing the VDQ method. It was assumed that the material properties of nanotube-reinforced composite are continuously varied through the thickness direction of conical shell and the temperature-dependent material properties were taken into account. Considering first-order shear deformation theory and Sander's strain-displacement relations, the energy functional were derived. The GDQ method in axial direction and periodic differential operators in circumferential direction were used to discretize the energy functional. The accuracy of the present numerical method was first validated with the results given in the literature. Furthermore, the effects of various parameters such as volume fractions and distributions of CNT, boundary conditions and semi-apex angles were examined on buckling and vibration of CNTRC thermally pre-stressed conical shells. As observed, temperature dependency of the material properties has significant effects on the mechanical behavior of FG-CNTRC conical shells under thermal loading so that considering the temperature-dependent material properties results in lower buckling temperatures. Also, it was found that the increase in volume fractions of CNTs increases the non-dimensional frequencies of nanocomposite conical shell, whereas this result is not correct for thermal buckling temperature. Symmetric distributions of CNTs along the thickness of the shell may lead to higher thermal buckling capacity and natural frequency. In addition, increase in length and vertex angle of conical shell makes it more flexible and declines the buckling temperature and fundamental frequency. Studying the effects of boundary conditions on dimensionless natural frequency of CNTRC conical shell revealed that considering the stiffer boundary conditions at edge of conical shell increases the buckling temperature and fundamental frequency. Generally, initial thermal loading decreases the non-dimensional natural frequency of FG-CNTRC conical shell. Additionally, it was observed that geometrical parameters of conical shell such as length-to-small radius and small radius-to-thickness ratio have an important role on vibration and buckling mode shapes.

References

Akbari, M., Kiani, Y. and Eslami, M.R. (2015), "Thermal buckling of temperature-dependent FGM conical shells with arbitrary edge supports", *Acta Mech*., **226**(3), 897-915.

Akgoz, B. and Civalek, O. (2013), "Buckling analysis of linearly tapered micro-columns based on strain gradient elasticity", *Struct. Eng. Mech*., **48**(2), 195-205.

Ansari, R. and Torabi, J. (2016), "Numerical study on the buckling and vibration of functionally graded carbon nanotube-reinforced composite conical shells under axial loading", *Compos. Part B: Eng*., **95**, 196-208.

Ansari, R., Torabi, J. and Shakouri, A.H. (2017a), "Vibration analysis of functionally graded carbon nanotube-reinforced composite elliptical plates using a numerical strategy", *Aerosp. Sci. Technol*., **60**, 152-161.

Ansari, R., Torabi, J. and Shojaei, M.F. (2017b), "Buckling and vibration analysis of embedded functionally graded carbon nanotube-reinforced composite annular sector plates under thermal loading", *Compos. Part B: Eng.*, **109**, 197-213.

Ansari, R., Torabi, J. and Shojaei, M.F. (2016), "Vibrational analysis of functionally graded carbon nanotube-reinforced composite spherical shells resting on elastic foundation using the variational differential quadrature method", *Eur. J. Mech.-A/Sol.*, **60**, 166-182.

Baltacıoğlu, A.K., Akgöz, B. and Civalek, Ö. (2010), "Nonlinear static response of laminated composite plates by discrete singular convolution method", *Compos. Struct.*, **93**(1), 153-161.

Baltacıoğlu, A.K., Civalek, Ö., Akgöz, B. and Demir, F. (2011), "Large deflection analysis of laminated composite plates resting on nonlinear elastic foundations by the method of discrete singular convolution", *Int. J. Press. Vess. Pip.*, **88**(8-9), 290-300.

Civalek, Ö. (2008), "Analysis of thick rectangular plates with symmetric cross-ply laminates based on first-order shear deformation theory", *J. Compos. Mater.*, **42**(26), 2853-2867.

Civalek, Ö., Korkmaz, A. and Demir, Ç. (2010), "Discrete singular convolution approach for buckling analysis of rectangular Kirchhoff plates subjected to compressive loads on two-opposite edges", *Adv. Eng. Softw.*, **41**(4), 557-560.

Esawi, A.M. and Farag, M.M. (2007), "Carbon nanotube reinforced composites: Potential and current challenges", *Mater. Des.*, **28**(9), 2394-2401.

Fiedler, B., Gojny, F.H., Wichmann, M.H., Nolte, M.C. and Schulte, K. (2006), "Fundamental aspects of nano-reinforced composites", *Compos. Sci. Technol.*, **66**(16), 3115-3125.

Gürses, M., Akgöz, B. and Civalek, Ö. (2012), "Mathematical modeling of vibration problem of nano-sized annular sector plates using the nonlocal continuum theory via eight-node discrete singular convolution transformation", *Appl. Math. Comput.*, **219**(6), 3226-3240.

Gürses, M., Civalek, Ö., Korkmaz, A.K. and Ersoy, H. (2009), "Free vibration analysis of symmetric laminated skew plates by discrete singular convolution technique based on first-order shear deformation theory", *Int. J. Numer. Meth. Eng.*, **79**(3), 290-313.

Heydarpour, Y., Aghdam, M.M. and Malekzadeh, P. (2014), "Free vibration analysis of rotating functionally graded carbon nanotube-reinforced composite truncated conical shells", *Compos. Struct.*, **117**, 187-200.

Ho, Y.H., Chang, C.P., Shyu, F.L., Chen, R.B., Chen, S.C. and Lin, M.F. (2004), "Electronic and optical properties of double-walled armchair carbon nanotubes", *Carb.*, **42**(15), 3159-3167.

Hosseini, S.M. (2013), "Application of a hybrid mesh-free method based on generalized finite difference (GFD) method for natural frequency analysis of functionally graded nanocomposite cylinders reinforced by carbon nanotubes", *CMES-Comput. Model Eng. Sci.*, **95**, 1-29.

Iijima, S. (1991), "Helical microtubules of graphitic carbon", *Nat.*, **354**(6348), 56.

Jin, G., Ye, T., Ma, X., Chen, Y., Su, Z. and Xie, X. (2013), "A unified approach for the vibration analysis of moderately thick composite laminated cylindrical shells with arbitrary boundary conditions", *Int. J. Mech. Sci.*, **75**, 357-376.

Kiani, Y. (2016), "Free vibration of functionally graded carbon nanotube reinforced composite plates integrated with piezoelectric layers", *Comput. Math. Appl.*, **72**(9), 2433-2449.

Kiani, Y. (2018), "Torsional vibration of functionally graded carbon nanotube reinforced conical shells", *Sci. Eng. Compos. Mater.*, **25**(1), 41-52.

Lam, D.C., Yang, F., Chong, A.C.M., Wang, J. and Tong, P. (2003), "Experiments and theory in strain gradient elasticity", *J. Mech. Phys. Sol.*, **51**(8), 1477-1508.

Liew, K.M., He, X.Q., Tan, M.J. and Lim, H.K. (2004), "Dynamic analysis of laminated composite plates with piezoelectric sensor/actuator patches using the FSDT mesh-free method", *Int. J. Mech. Sci.*, **46**(3), 411-431.

Manchado, M.L., Valentini, L., Biagiotti, J. and Kenny, J.M. (2005), "Thermal and mechanical properties of single-walled carbon nanotubes-polypropylene composites prepared by melt processing", *Carb.*, **43**(7), 1499-1505.

Mehrabadi, S.J. and Aragh, B.S. (2014), "Stress analysis of functionally graded open cylindrical shell reinforced by agglomerated carbon nanotubes", *Thin-Wall. Struct.*, **80**, 130-141.

Mirzaei, M. and Kiani, Y. (2015), "Thermal buckling of temperature dependent FG-CNT reinforced composite conical shells", *Aerosp. Sci. Technol.*, **47**, 42-53.

Mohammadimehr, M. and Alimirzaei, S. (2016), "Nonlinear static and vibration analysis of Euler-Bernoulli composite beam model reinforced by FG-SWCNT with initial geometrical imperfection using FEM", *Struct. Eng. Mech.*, **59**(3), 431-454.

Oñate, E. (2013), *Structural Analysis with the Finite Element Method. Linear Statics: Volume 2: Beams, Plates and Shells*, Springer Science and Business Media.

Raminnea, M., Biglari, H. and Tahami, F.V. (2016), "Nonlinear higher order Reddy theory for temperature-dependent vibration and instability of embedded functionally graded pipes conveying fluid-nanoparticle mixture", *Struct. Eng. Mech.*, **59**(1), 153-186.

Shen, H.S. (2009), "Nonlinear bending of functionally graded carbon nanotube-reinforced composite plates in thermal environments", *Compos. Struct.*, **91**(1), 9-19.

Shen, H.S. (2012), "Thermal buckling and postbuckling behavior of functionally graded carbon nanotube-reinforced composite cylindrical shells", *Compos. Part B: Eng.*, **43**(3), 1030-1038.

Shen, H.S. and Xiang, Y. (2012), "Nonlinear vibration of nanotube-reinforced composite cylindrical shells in thermal environments", *Comput. Meth. Appl. Mech. Eng.*, **213**, 196-205.

Shen, H.S. and Xiang, Y. (2014), "Nonlinear vibration of nanotube-reinforced composite cylindrical panels resting on elastic foundations in thermal environments", *Compos. Struct.*, **111**, 291-300.

Shen, H.S. and Xiang, Y. (2015), "Thermal postbuckling of nanotube-reinforced composite cylindrical panels resting on elastic foundations", *Compos. Struct.*, **123**, 383-392.

Shen, H.S. and Zhang, C.L. (2010), "Thermal buckling and postbuckling behavior of functionally graded carbon nanotube-reinforced composite plates", *Mater. Des.*, **31**(7), 3403-3411.

Shojaei, M.F. and Ansari, R. (2017), "Variational differential quadrature: A technique to simplify numerical analysis of structures", *Appl. Math. Modell.*, **49**, 705-738.

Sofiyev, A.H., Keskin, E.M., Erdem, H. and Zerin, Z. (2003), "Buckling of an orthotropic cylindrical thin shell with continuously varying thickness under a dynamic loading", *Ind. J. Eng. Mater. Sci.*, **10**, 365-370.

Sofiyev, A. H., Zerin, Z., Allahverdiev, B.P., Hui, D., Turan, F. and Erdem, H. (2017b), "The dynamic instability of FG orthotropic conical shells within the SDT", *Steel Compos. Struct.*, **25**(5), 581-591.

Sofiyev, A.H., Zerin, Z. and Kuruoglu, N. (2017a), "Thermoelastic buckling of FGM conical shells under non-linear temperature rise in the framework of the shear deformation theory", *Compos. Part B: Eng.*, **108**, 279-290.

Sumfleth, J., Prehn, K., Wichmann, M.H., Wedekind, S. and Schulte, K. (2010), "A comparative study of the electrical and mechanical properties of epoxy nanocomposites reinforced by CVD-and arc-grown multi-wall carbon nanotubes", *Compos. Sci. Technol.*, **70**(1), 173-180.

Talebitooti, M. (2013), "Three-dimensional free vibration analysis of rotating laminated conical shells: Layerwise differential

quadrature (LW-DQ) method", *Arch. Appl. Mech.*, **83**(5), 765-781.
Torabi, J., Kiani, Y. and Eslami, M.R. (2013), "Linear thermal buckling analysis of truncated hybrid FGM conical shells", *Compos. Part B: Eng.*, **50**, 265-272.
Tornabene, F., Viola, E. and Inman, D.J. (2009), "2-D differential quadrature solution for vibration analysis of functionally graded conical, cylindrical shell and annular plate structures", *J. Sound Vibr.*, **328**(3), 259-290.
Xiang, Y., Ma, Y. F., Kitipornchai, S., Lim, C.W. and Lau, C.W.H. (2002), "Exact solutions for vibration of cylindrical shells with intermediate ring supports", *Int. J. Mech. Sci.*, **44**(9), 1907-1924.
Yakobson, B.I. and Avouris, P. (2001), *Mechanical Properties of Carbon Nanotubes. In Carbon Nanotubes (pp. 287-327)*, Springer, Berlin, Heidelberg, Germany.
Yang, J., Ke, L.L. and Feng, C. (2015), "Dynamic buckling of thermo-electro-mechanically loaded FG-CNTRC beams", *Int. J. Struct. Stab. Dyn.*, **15**(8), 1540017.
Yas, M.H., Pourasghar, A., Kamarian, S. and Heshmati, M. (2013), "Three-dimensional free vibration analysis of functionally graded nanocomposite cylindrical panels reinforced by carbon nanotube", *Mater. Des.*, **49**, 583-590.
Zhang, L.W., Song, Z.G. and Liew, K.M. (2016), "Computation of aerothermoelastic properties and active flutter control of CNT reinforced functionally graded composite panels in supersonic airflow", *Comput. Meth. Appl. Mech. Eng.*, **300**, 427-441.

CC

Appendix: Computation of shear correction factors

The shear correction factor can be computed by matching the shear strain energy obtained for an exact 3D distribution of the transverse shear stresses τ_{23} and τ_{13} (denotes by U_1) and shear strain energy related to the first-order shear deformation theory (denotes by U_2). Considering the stress vector, the shear strain energy for 3D model can be given as (Oñate 2013)

$$U_1 = \frac{1}{2}\int_{-h/2}^{h/2} \boldsymbol{\sigma}_s^{\mathrm{T}} \mathbf{C}_s^{-1} \boldsymbol{\sigma}_s dz \tag{A-1}$$

and for the first-order shear deformation plate theory

$$U_2 = \frac{1}{2}\mathbf{N}_s^{\mathrm{T}} \hat{\mathbf{C}}_s^{-1} \mathbf{N}_s \tag{A-2}$$

where

$$\mathbf{N}_s = \int_{-h/2}^{h/2} \boldsymbol{\sigma}_s dz \tag{A-3}$$

In the above equations, $\mathbf{N}_s$ presents the vector of transverse force resultants. Furthermore, $\mathbf{C}_s$ and $\hat{\mathbf{C}}_s$ were defined in Eqs. (22) and (27) respectively. Matching U_1 and U_2 results in the expression for $\bar{\mathbf{C}}_s$ and accordingly, the transverse shear correction factors can be obtained. On the basis of the analytical approach outlined in (Oñate 2013), by the use of equilibrium equations of 3D elasticity and considering some assumptions, Eq. (A-1) can be represented as

$$U_1 \cong \frac{1}{2}\mathbf{N}_s^{\mathrm{T}} \mathbf{H}_s \mathbf{N}_s \tag{A-4}$$

with

$$\mathbf{H}_s = \int_{-h/2}^{h/2} \mathbf{Q}^{\mathrm{T}} \mathbf{C}_s^{-1} \mathbf{Q}\, dz \tag{A-5}$$

$$\mathbf{Q} = \int_{-h/2}^{z} \frac{z}{2} \begin{bmatrix} A_{11}+A_{33} & A_{13}+A_{32} \\ A_{31}+A_{32} & A_{22}+A_{33} \end{bmatrix} dz \tag{A-6}$$

Where A_{ij} are the components of matrix $\mathbf{A}$ defined as

$$\mathbf{A} = \mathbf{C}_p \bar{\mathbf{C}}_p^{-1}, \qquad \bar{\mathbf{C}}_p = \int_{-\frac{h}{2}}^{\frac{h}{2}} z^2 \mathbf{C}_p dz \tag{A-7}$$

By equaling U_1 (Eq. (A-4)) and U_2 (Eq. (A-2)), the generalized transverse shear strain constitutive matrix is obtained as

$$\hat{\mathbf{C}}_s = \mathbf{H}_s^{-1} = \hat{\mathbf{H}}_s \tag{A-8}$$

According to Eq. (A-8) and considering Eq. (27), the shear correction factors are determined as

$$\kappa_{11} = \frac{\hat{H}_{s_{11}}}{\hat{C}_{s_{11}}}, \qquad \kappa_{22} = \frac{\hat{H}_{s_{22}}}{\hat{C}_{s_{22}}} \tag{A-9}$$

where $\hat{H}_{s_{ij}}$ are the components of $\hat{\mathbf{H}}_s = \mathbf{H}_s^{-1}$ and $\hat{C}_{s_{ij}}$ are defined in Eq. (27).